



Published in final edited form as:

J Am Chem Soc. 2020 September 02; 142(35): 14877–14889. doi:10.1021/jacs.0c02810.

Higher Magnetic Fields, Finer MOF Structural Information: ^{17}O Solid-State NMR at 35.2 T

Vinicius Martins^{#‡}, Jun Xu^{#§,*}, Xiaoling Wang[§], Kuizhi Chen[§], Ivan Hung[§], Zhehong Gan^{§,*}, Christel Gervais[#], Christian Bonhomme^{#,*}, Shijia Jiang[§], Anmin Zheng[§], Bryan E.G. Lucier[‡], Yining Huang^{‡,*}

[‡]Department of Chemistry, The University of Western Ontario, 1151 Richmond Street, London, ON, N6A 5B7, Canada

[§]Center for Rare Earth and Inorganic Functional Materials, Tianjin Key Lab for Rare Earth Materials and Applications, School of Materials Science and Engineering & National Institute for Advanced Materials, Nankai University, Tianjin 300350, P.R. China

[§]National High Magnetic Field Laboratory (NHMFL), 1800 East Paul Dirac Dr., Tallahassee, FL 32310, USA

[#]Sorbonne Université, CNRS, UMR 7574, Laboratoire de Chimie de la Matière Condensée de Paris, LCMCP, F-75005 Paris, France

[§]State Key Laboratory of Magnetic Resonance and Atomic and Molecular Physics, Wuhan Institute of Physics and Mathematics, Innovation Academy for Precision Measurement Science and Technology, Chinese Academy of Sciences, Wuhan 430071, P. R. China

[#] These authors contributed equally to this work.

Abstract

The spectroscopic study of oxygen, a vital element in materials, physical, and life sciences, is of tremendous fundamental and practical importance. ^{17}O solid-state NMR (SSNMR) spectroscopy has evolved into an ideal site-specific characterization tool, furnishing valuable information on the local geometric and bonding environments about chemically distinct and, in some favorable cases, crystallographically inequivalent oxygen sites. However, ^{17}O is a challenging nucleus to study via SSNMR, as it suffers from low sensitivity and resolution, owing to the quadrupolar interaction and low ^{17}O natural abundance. Herein, we report a significant advance in ^{17}O SSNMR spectroscopy. ^{17}O isotopic enrichment and the use of an ultrahigh 35.2 T magnetic field has unlocked identification of many inequivalent carboxylate oxygen sites in the as-made and activated phases of the metal–organic framework (MOF) $\alpha\text{-Mg}_3(\text{HCOO})_6$. The subtle ^{17}O spectral differences between the as-made and activated phases yield detailed information about host–guest interactions, including insight into nonconventional O...H—C hydrogen bonding. Such weak interactions often play key roles in applications of MOFs, such as gas adsorption and biomedicine,

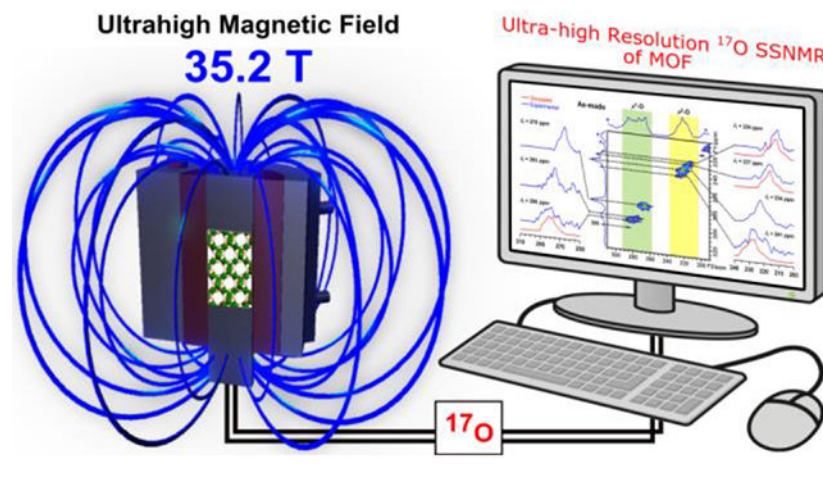
*Corresponding Author junxu@nankai.edu.cn; gan@magnet.fsu.edu; christian.bonhomme@upmc.fr; yhuang@uwo.ca.

Supporting Information.

Powder XRD patterns, TGA profiles, and ^1H – ^{13}C CP/MAS NMR spectra of $\alpha\text{-Mg}_3(\text{HCOO})_6$, experimental details on ^{17}O -enriched MIL-53(Al) preparation and the powder XRD patterns of this MOF, additional NMR data and analyses. The Supporting Information is available free of charge on the ACS Publications website.

and are usually difficult to study via other characterization routes. The power of performing ^{17}O SSNMR experiments at ultrahigh magnetic field of 35.2 T for MOF characterization is further demonstrated by examining activation of the MIL-53(Al) MOF. The sensitivity and resolution enhanced at 35.2 T allows partially- and fully-activated MIL-53(Al) to be unambiguously distinguished, and also permits several oxygen environments in the partially-activated phase to be tentatively identified. This demonstration of the very high resolution of ^{17}O SSNMR recorded at the highest magnetic field accessible to chemists to date illustrates how a broad variety of scientists can now study oxygen-containing materials and obtain previously inaccessible fine structural information.

Graphical Abstract



1. Introduction

The element of oxygen is ubiquitous across nearly all scientific fields. Therefore, characterization of oxygen local electronic and geometric environments is very important. ^{17}O solid-state NMR (SSNMR) spectroscopy has become an ideal site-specific characterization tool for probing oxygen local environments, as ^{17}O is sensitive to the chemical shift and quadrupolar interactions,¹⁻¹¹ has a large diagnostic chemical shift range,¹²⁻²⁵ and is influenced by coupling to neighboring NMR-active nuclei (*e.g.*, ^1H , ^{13}C , and ^{15}N).²⁶⁻³¹ There has been tremendous progress made in NMR methodology and technology in recent years, yet the potential of ^{17}O SSNMR for uncovering detailed structural and bonding information in oxygen-containing compounds has been limited by the inherently low sensitivity and resolution resulting from the very low natural abundance (0.038%), relatively low gyromagnetic ratio ($\gamma = -5.774 \text{ MHz}\cdot\text{T}^{-1}$), and quadrupolar nature (spin $I = 5/2$) of ^{17}O .³²

The sensitivity problem associated with the low ^{17}O natural abundance can be mitigated by isotopic enrichment.¹⁶⁻²² To address the relatively low γ and quadrupolar nature of ^{17}O , NMR measurements can be performed at high magnetic fields; this not only inherently enhances sensitivity but also reduces spectral line broadening associated with the second-order quadrupolar interaction. A new series-connected resistive/superconducting hybrid

magnet operating at a record-high magnetic field strength of 35.2 T (^1H Larmor frequency of 1.5 GHz) has recently entered service,³³ which promises very high ^{17}O SSNMR resolution in biomolecules and minerals.³³⁻³⁵ In this work, taking advantage of the state-of-the-art magnet and *rf* technology, we targeted microporous $\alpha\text{-Mg}_3(\text{HCOO})_6$ to demonstrate that very high spectral resolution of ^{17}O SSNMR spectra can be achieved at 35.2 T, providing an excellent opportunity for characterizing promising materials such as metal-organic frameworks (MOFs).

MOFs are a fascinating family of hybrid organic-inorganic porous materials with many practical applications.³⁶⁻³⁷ SSNMR spectroscopy of MOFs has proven to be a powerful tool for characterizing the immediate environment about metal centers and probing the local structure of organic linkers.³⁸⁻⁴⁰ SSNMR can also provide information on the behavior of adsorbed guests, which is critically important for many applications.⁴¹⁻⁴² For example, MOFs are promising materials for the removal of greenhouse gas such as CO_2 and storage of fuels such as H_2 and CH_4 . SSNMR can provide information on the location of guest species,^{10, 43-47} which is critically important for practical applications, as the location of guest gas molecules can be directly linked to binding site positions and strength, respectively. Similarly, ascertaining the location of guest species in MOFs is key to understanding their applications in sensing and drug delivery.⁴⁸⁻⁵¹ Oxygen present in various carboxylate ligands, which are the most extensively used organic linkers, is a key constituent of many important MOFs.⁵²⁻⁵⁶ Oxygen anions (O^{2-}) are also associated with the metal clusters of the frameworks (e.g., MOF-5).⁵² Hydroxyl groups are common linkers bridging metal clusters (e.g., MIL-53)⁵³ and exist as part of the secondary building units (e.g., UiO-66).⁵⁴ Water molecules can directly bond to the metal center, with well-known examples include as-made MOF-74 and HKUST-1.⁵⁵⁻⁵⁶ These oxygen species play critical roles in applications such as guest adsorption/separation,⁵⁷ sensing,⁴⁸ catalysis,⁵⁸ solid-state conductors,⁵⁹ and biomedicine,⁴⁹⁻⁵¹ rendering oxygen a key target for MOF characterization. Although ^{17}O SSNMR has been utilized to examine some MOFs,^{10, 15-17} potential successes in molecular-level characterization and site assignment have been limited by spectral resolution.

Microporous $\alpha\text{-Mg}_3(\text{HCOO})_6$ is an attractive target for ^{17}O SSNMR characterization for several reasons.

- i. Microporous $\alpha\text{-Mg}_3(\text{HCOO})_6$ is a commercially available and low-cost MOF with good molecular selectivity, such as a preference for C_2H_2 over CO_2 .⁶⁰⁻⁶¹ It is a representative small pore MOF suitable for gas adsorption.
- ii. This MOF presents a very challenging case for characterization by ^{17}O SSNMR, as the crystal structure features twelve inequivalent carboxylate oxygen sites across two bonding modes. Using our highest available field of 21.1 T at the time, only two ^{17}O NMR signals corresponding to the two different oxygen bonding modes of formate anions could be observed (*vide infra*).¹⁶ As increasing the magnetic field from 21.1 to 35.2 T leads to an improvement in resolution by a factor of 2.8 (the second-order quadrupolar broadening in ppm varies as the inverse ratio of the fields squared),¹ resolving many of these inequivalent oxygen sites at 35.2 T should be possible.

- iii. The applications of MOFs require the removal of the solvent molecules from inside the pores of as-made MOFs in a process known as “activation”. Activation often leads to changes in the framework structure. While significant changes can be detected by X-ray diffraction, activation-induced changes for MOFs including α -Mg₃(HCOO)₆ can be subtle (i.e., small changes in unit cell parameters), and the specific molecular-level alterations cannot be detected by diffraction-based methods. Thus, it is important to develop SSNMR as a method complementary to XRD. The high spectral resolution that can be achieved at 35.2 T holds promise for providing fine details on oxygen local environments, reflecting the changes resulting from activation.
- iv. MOFs have many potential applications across fields such as biology and medicine.⁶²⁻⁶³ Thus, nonconventional O...H—C hydrogen bonding involving guest species and bioactive components in the framework can play important roles for host–guest interactions in BioMOFs, a new subclass of MOFs,⁴⁹⁻⁵⁰ or MOF-based drug delivery systems.⁵¹ Since nonconventional O...H—C hydrogen bonding has been observed in as-made α -Mg₃(HCOO)₆ (C₆H₆Mg₃O₁₂·C₃H₇NO, C₃H₇NO is *N,N'*-dimethylformamide or DMF),⁶⁴ this system has been selected as a model compound to explore the possibility of using ¹⁷O SSNMR at 35.2 T to directly probe this weak host–guest interaction in MOF systems.

Our results show that the ¹⁷O SSNMR spectra of α -Mg₃(HCOO)₆ samples acquired at 35.2 T indeed exhibit very high resolution, allowing many inequivalent framework oxygen sites to be identified. The high resolution and sensitivity realized at 35.2 T not only lead to ultrafine information on oxygen local environment and corresponding subtle changes upon activation, but also make it possible to detect weak host–guest interactions such as nonconventional O...H—C hydrogen bonding. To further illustrate the benefits of performing ¹⁷O SSNMR at an ultrahigh field of 35.2 T, we examined two activated MOF MIL-53(Al) samples; the high spectral resolution and sensitivity allow us to unambiguously distinguish partially-activated from fully-activated MIL-53(Al) samples. The very high resolution and sensitivity of ¹⁷O SSNMR achievable at 35.2 T detailed in this work illustrates the great potential of SSNMR for unlocking fine structural information in solids as higher magnetic fields become increasingly available.

2. Experimental Methods

2.1. Synthesis and characterization of MOF samples.

As-made ¹⁷O-enriched α -Mg₃(HCOO)₆ was synthesized according to the reported procedure.¹⁶ The starting materials were used as received without further purification. A mixture of Mg(NO₃)₂·6H₂O (3 mmol, Aldrich) and HCOOH (6 mmol, Aldrich) was dissolved in 10 mL of DMF and 0.25 mL of ¹⁷O-enriched H₂O (6 mmol, CortecNet, 35 atom%) in a 23 mL Teflon-lined autoclave. The container was sealed and heated at 383 K for 2 days. After cooling the autoclave to room temperature, the white powder product was collected, washed with DMF and dried overnight at 363 K. Activated ¹⁷O-enriched α -Mg₃(HCOO)₆ was obtained by heating as-made ¹⁷O-enriched α -Mg₃(HCOO)₆ at 423 K

overnight under dynamic vacuum. The PXRD patterns of ^{17}O -enriched $\alpha\text{-Mg}_3(\text{HCOO})_6$ samples are shown in Figure S1, Supporting Information (SI).

In the experimental PXRD patterns of as-made and activated $\alpha\text{-Mg}_3(\text{HCOO})_6$, the two low angle reflections at $2\theta = 9.7^\circ$ ($-1\ 0\ 1$) and 9.9° ($1\ 0\ 1$) are much weaker than the reflection at 10.7° ($0\ 1\ 1$), which strays from the comparable intensities apparent in the simulated PXRD spectra. A previous study demonstrated that the PXRD patterns of $\alpha\text{-Mg}_3(\text{HCOO})_6$ crystals prepared under different synthetic conditions may exhibit different intensity patterns.⁶⁵ In particular, the three low-angle reflections at 9.7° , 9.9° , and 10.7° have different relative intensities if water is involved. For $\alpha\text{-Mg}_3(\text{HCOO})_6$ samples prepared in the presence of water, the relative intensity pattern for the three above-mentioned low-angle diffractions looks very similar to that seen in Figure S1, but distinct from the simulated PXRD pattern based on the structure determined from a single crystal prepared in non-aqueous DMF solvent.⁶⁰ In the present work, ^{17}O -enriched $\alpha\text{-Mg}_3(\text{HCOO})_6$ was prepared in the presence of ^{17}O -enriched H_2O . Although the synthesis of $\alpha\text{-Mg}_3(\text{HCOO})_6$ is very straightforward and highly reproducible, and we have made this MOF routinely in many studies with and without water,^{16, 43-46, 64, 66-68} to unambiguously confirm the identity of the samples used in the present study we repeated the sample preparation several times. These additional samples were prepared under the exact same conditions used for preparing ^{17}O -enriched MOF, except that normal water was used rather than ^{17}O -enriched water. Figure S1 indicates that when the samples were prepared in the presence of a small amount of water, the relative intensities of the first two low-angle reflections are significantly lower than that of the third one, which is consistent with the literature.⁶⁵ We performed a Le Bail fit of the PXRD data using the GSAS II package (Figure S2, see the SI for details),⁶⁹ and obtained unit cell parameters of the samples prepared in the presence of water that are comparable to those reported in the literature (Table S1); this data indicates that although the relative intensities of reflections may differ, the samples indeed share the same crystal structure.

The activation process for this MOF has been proven to be robust.^{60, 64, 66, 70} To verify the solvent DMF molecules occluded inside the channels are completely removed upon activation, TGA profiles and ^1H - ^{13}C CP/MAS SSNMR spectra were obtained (Figure S3 and S4, with experimental details in Section S2). The results unanimously agree that the activation process is very effective and the solvent molecules are completely removed.

The synthesis of ^{17}O -enriched MIL-53(Al) samples and corresponding PXRD patterns (Figure S5) can be found in Section S3 of the Supporting Information.

2.2. ^{17}O solid-state NMR measurements.

The 1D rotor-synchronized spin-echo spectrum of activated $\alpha\text{-Mg}_3(\text{HCOO})_6$ was recorded at 21.1 T (^{17}O Larmor frequency of 122.0 MHz) on a Bruker Avance II spectrometer at the National Ultrahigh-Field NMR Facility for Solids in Ottawa, Canada. A 4 mm H/X MAS Bruker probe and a spinning frequency of 18 kHz were used. The recycle delay was 4 s. A $\pi/2$ pulse of 4 μs was used.

1D and 2D ^{17}O SSNMR experiments at 35.2 T were performed on the series-connected hybrid (SCH) magnet (^{17}O Larmor frequency of 203.4 MHz) at the National High Magnetic

Field Laboratory (NHMFL) in Tallahassee, USA.³³ A Bruker Avance NEO console and a NHMFL home-built single-resonance 3.2 mm low-gamma MAS probe were used, along with a spinning frequency of 18 kHz and a pulse delay of 0.1 s. The pulse delay was optimized to achieve the highest S/N and no significant changes in NMR lineshapes were observed when employing different pulse delays. A $\pi/2$ pulse of 5.0 μs was used in 1D rotor-synchronized spin echo experiments. All rotor-synchronized 3QMAS spectra were acquired using the shifted-echo pulse sequence.⁷¹ The 3Q excitation and conversion pulses were 3.0 and 1.0 μs , respectively. The number of t_1 increments was 34. Since the shifted-echo is phase modulated, the number of time increments was also 34, corresponding to a maximum t_1 evolution time of ~ 1.9 ms. Note that during spectral acquisition, the number of t_1 increments were carefully chosen to include a significant portion beyond the point where the signal dropped to the baseline noise level, ensuring that the shifted-echo 3QMAS spectra were acquired with the highest S/N during the limited SCH magnet time without compromising the resolution. The 3QMAS spectra were acquired using rotor-synchronized t_1 increments to avoid spinning sidebands, which are significant due to the chemical shift anisotropy (CSA) at the very high field and 3Q excitation/conversion modulation along the indirect F1 dimension. However, this restricts the F1 window to the spinning frequency (18 kHz), which is not wide enough to cover the spread of resonances and spinning side bands (SSBs). Fortunately, this problem can be solved by the Q-shearing method to the $k = 3$ Q-representation.⁷² The F1 spectral window can then be zero-filled and expanded to whatever limits are needed for shearing back to the isotropic representation with a large and unfolded F1 window. In the present case, the F1 spectral window was zero-filled eight times and expanded to give an unfolded F1 window of 8×18 kHz after Q-shearing. Consequently, the F1 digital resolution is equivalent to 8×34 t_1 increments with the final expanded F1 window. The ^{17}O spectra were referenced to 18 atom% ^{17}O -enriched $\text{H}_2^{17}\text{O}(\text{l})$ or distilled water at 0 ppm.

2.3. Spectral simulations.

For quadrupolar nuclei such as ^{17}O (spin $I > 1/2$), their electric quadrupole moments interact with the surrounding EFG, resulting in broad powder patterns rather than sharper resonances. The interplay between the quadrupolar interaction with the CSA effect makes the shapes of powder patterns more complicated and difficult to simulate. The dmfit software package was used to simulate SSNMR spectra using the Int2QUAD mode, including both the quadrupolar and CSA effects.⁷³ In dmfit, the EFG tensor is described by three principal components in the following order: $|V_{YY}|$ $|V_{XX}|$ $|V_{ZZ}|$. The quadrupolar coupling constant (C_Q) and asymmetry parameter (η_Q) describe the spherical and cylindrical symmetry of the EFG tensor, respectively, and are defined as follows: $C_Q = (eQV_{ZZ}/h) \times 9.7177 \times 10^{21}$ (in Hz) and $\eta_Q = (V_{YY} - V_{XX})/V_{ZZ}$, where e is the electric charge, Q is the quadrupole moment ($-2.558 \times 10^{-30} \text{ m}^2$),³² and a conversion factor of $9.7177 \times 10^{21} \text{ V}\cdot\text{m}^{-2}$ is used during the calculation of C_Q to convert from atomic units to Hz. The chemical shift (CS) tensor is also described by three principal components such that $|\delta_{22} - \delta_{\text{iso}}|$ $|\delta_{11} - \delta_{\text{iso}}|$ $|\delta_{33} - \delta_{\text{iso}}|$, and the isotropic chemical shift $\delta_{\text{iso}} = (\delta_{11} + \delta_{22} + \delta_{33})/3$ relates to the bonding modes. The CSA parameters are defined by $\eta_{\text{CS}} = (\delta_{22} - \delta_{11})/|\text{CS}|$ and $\eta_{\text{CS}} = (\delta_{22} - \delta_{11})/|\text{CS}|$. Three Euler angles (ϕ , χ , ψ) are employed to describe the orientations of the CS tensor with respect to the EFG principal (fixed) axis frame using the ZYZ convention: the

corresponding transformation matrix was used to deduce the new directional characteristics of the CS tensor with respect to the EFG system. As a result, eight independent parameters, C_Q , η_Q , δ_{iso} , C_S , η_{CS} , ϕ , χ , and ψ are required to characterize a single ^{17}O site when both the quadrupolar and the CSA effects are considered. All uncertainties in NMR parameters were estimated by bidirectional variation of the parameter of interest in both directions from the best-fit value while holding all other NMR parameters constant.

2.4. Theoretical calculations.

The unit cell parameters were set to the single-crystal XRD parameters⁶⁰ and kept fixed during geometry optimizations to ensure consistency between experimental and optimized structures. Proton positions were then optimized using the VASP (Vienna Ab-initio Simulation Package) code⁷⁴ based on the Kohn-Sham Density Functional Theory (DFT) and using a plane-wave pseudopotential approach. The NMR parameters were then calculated within Kohn-Sham DFT using the QUANTUM-ESPRESSO code.⁷⁵ The PBE generalized gradient approximation⁷⁶ was used and the valence electrons were described by norm-conserving pseudopotentials⁷⁷ in the Kleinman Bylander form.⁷⁸ The wave functions were expanded on a plane wave basis set with a kinetic energy cut-off of 80 Ry. The integral over the first Brillouin zone was performed using a Monkhorst-Pack $2 \times 2 \times 2$ k-point grid for the charge density and chemical shift tensor calculation. The magnetic shielding tensor was computed using the Gauge-Including Projector Augmented Wave (GIPAW) approach,⁷⁹⁻⁸¹ which enables the reproduction of the results of a fully converged all-electron calculation. The isotropic chemical shift δ_{iso} is defined as $\delta_{\text{iso}} = [\sigma_{\text{iso}} - \sigma_{\text{iso}(\text{ref})}]$, where σ_{iso} is the isotropic magnetic shielding and $\sigma_{\text{iso}(\text{ref})}$ is the isotropic magnetic shielding of the same nucleus in a reference compound. In the present case, the fit of the linear correlation between the experimental δ_{iso} and the calculated σ_{iso} values of ^{17}O for Na_2SiO_3 , α - $\text{Na}_2\text{Si}_2\text{O}_5$, α - and γ -glycine, and α - SrSiO_3 enabled the determination of the relation between δ_{iso} and calculated σ_{iso} for the ^{17}O nucleus, as described previously.²¹ It is worth noting that for most MOFs, the solvent molecules are disordered inside the framework. Very often, disordered solvent molecules have to be removed before calculation. In the present case, the DMF molecules are orderly distributed within the channels. This rare situation makes the calculation not only simpler, but also more accurate.

3. Results and Discussion

The three-dimensional framework of microporous α - $\text{Mg}_3(\text{HCOO})_6$ is formed by corner- and edge-sharing MgO_6 octahedra interconnected by formate ligands (Figure 1), and features zig-zag channels measuring $4.5 \times 5.5 \text{ \AA}$.⁶⁰ Among the twelve crystallographically distinct framework oxygen sites, six are associated with the carboxylate group and adopt a μ^2 -O bonding mode (sites O1, O3, O5, O7, O9, and O11), and the other six are associated with the carboxylate group and are in a μ^1 -O bonding mode (sites O2, O4, O6, O8, O10, and O12). The C— μ^1 -O bonds are of shorter length and more double-bond character than the C— μ^2 -O bonds. However, the local environments of all six μ^1 -O sites are almost identical, while the six μ^2 -O sites are also very similar. As a result, only two signal groups were resolved in previous ^{17}O 1D magic-angle spinning (MAS) spectrum of as-made α - $\text{Mg}_3(\text{HCOO})_6$ at 21.1 T (Figure 1).¹⁶ Those two ^{17}O signals were simulated reasonably well by two ^{17}O powder

patterns at 21.1 T and were assigned to groups of μ^1 - and μ^2 -O sites, respectively (Figure S6, Supporting Information).

As-made MOFs typically consist of solvent molecules occupying their pores and channels; thus the creation of permeable spaces in MOFs by evacuating the solvent (*i.e.*, the activation process) is a pre-requisite for many applications. Therefore, it is of fundamental importance to understand the effect of activation on the MOF structure, especially regarding the subtle local environment changes that are invisible in diffraction-based techniques but very important for applications. The single-crystal XRD data of as-made and activated α - $\text{Mg}_3(\text{HCOO})_6$ phases indicate that the local oxygen environments only undergo very minor changes upon removal of DMF solvent during activation, as the Mg ions are coordinately saturated and this MOF framework is fairly rigid.⁶⁰ Consequently, detecting the very small activation-induced structural changes via ^{17}O SSNMR is quite challenging, as evidenced by the nearly identical ^{17}O 1D MAS spectra of two phases at 21.1 T (Figure 1). It is apparent that higher spectral resolution is necessary to detect the subtle difference in oxygen local environment. The activation method employed in this work for DMF solvent removal from α - $\text{Mg}_3(\text{HCOO})_6$ is well established.^{60, 70} Based on our previous experience, we are certain that this activation process completely removes all residual DMF guests from the as-made MOF.^{64, 66} To confirm, we carried out TGA alongside ^1H — ^{13}C CP/MAS experiments, and the results unambiguously prove that the activation is complete (see Section S2 for details).

The newly-obtained ^{17}O 1D MAS NMR spectra of as-made and activated α - $\text{Mg}_3(\text{HCOO})_6$ phases at 35.2 T are shown in Figure 1 alongside the 21.1 T spectra. At 35.2 T, the resonances of both phases are considerably narrower, owing to the reduced second-order quadrupolar broadening. The spectral envelope containing all overlapping signals of the μ^1 -O group is now completely separated from that of the μ^2 -O group at 35.2 T, and several diagnostic spectral features including the “edges” and “horns” of individual ^{17}O SSNMR resonances have emerged. Thus, this spectral envelope must consist of several overlapping powder patterns corresponding to multiple μ^1 -O sites. Similarly, the spectral envelope of the μ^2 -O group should also be simulated using multiple powder patterns. However, due to the severe overlap of powder patterns, it is very challenging to determine the number of oxygen sites and their corresponding NMR parameters using only a 1D MAS spectrum. Furthermore, the ^{17}O 1D MAS spectra of as-made and activated α - $\text{Mg}_3(\text{HCOO})_6$ phases are now distinctly different at 35.2 T, implying that the activation-induced structural changes not apparent at 21.1 T are now discernable, owing to the much higher spectral resolution achieved at 35.2 T. It is worth mentioning that the changes in the μ^1 -O spectral envelope are also more significant than those in the μ^2 -O one, suggesting that the local environments of μ^1 -O sites are more influenced by activation versus μ^2 -O sites. The spectra exhibit very intense spinning sidebands due to the chemical shift anisotropy (CSA) enhanced at 35.2 T.

As mentioned earlier, the ^{17}O 1D MAS spectra at 35.2 T feature overlapping resonances arising from multiple ^{17}O sites, indicating that the maximum achievable 1D spectral resolution is still not high enough to resolve fine features. This is because the conventional 1D MAS experiments only partially averages the ^{17}O second-order quadrupolar interaction. To further enhance spectral resolution, 2D 3QMAS experiments were performed:⁸² this technique can eliminate the ^{17}O second-order quadrupolar broadening along the indirect F1

dimension and thus separate the overlapping signals observed in 1D MAS spectra. The ^{17}O 2D 3QMAS spectra of as-made and activated $\alpha\text{-Mg}_3(\text{HCOO})_6$ at 35.2 T are shown in Figure 2. There are a number of well-resolved signals along the F1 dimension in the spectra of the as-made and activated phases, respectively. Since the number of resolved signals in the isotropic dimension (seven for the as-made phase and eight for the activated phase) is smaller than the twelve crystallographically distinct framework oxygen sites, some signals along the F1 dimension must correspond to very similar signals arising from multiple oxygen sites with almost identical NMR parameters.

For each F2 cross-section extracted at δ_1 along the F1 dimension, the isotropic chemical shift, δ_{iso} (in ppm), and the quadrupolar product, $P_Q = C_Q(1 + \eta_Q^2/3)^{1/2}$ (in MHz), can be obtained directly from the spectral center of gravity (δ_2) along the F2 dimension¹⁷ using the following equations⁸³

$$\delta_{\text{iso}} = \frac{17}{27}\delta_1 + \frac{10}{27}\delta_2$$

$$P_Q = \left\{ \frac{170}{81} \frac{[4I(2I-1)]^2}{[4I(I+1)-3]} (\delta_1 - \delta_2) \right\}^{1/2} \nu_0 \times 10^{-3}$$

where ν_0 is the Larmor frequency and I is the spin quantum number.

The δ_{iso} and P_Q values derived from each peak along the F1 dimension are given in Table 1. These two values are determined accurately from the resonance positions in F1 and F2 dimensions, without the need of fitting the F2 cross-section, under the S/N obtained with the limited magnet time.

For the peaks along the isotropic dimension corresponding to a single oxygen site, C_Q and η_Q values can be extracted by fitting the F2 cross-section. If a peak along the F1 dimension originates from multiple oxygen sites, δ_{iso} and P_Q represent average values. To assign each resolved signal in the isotropic dimension to a single or multiple oxygen sites, gauge-including projector augmented wave (GIPAW) density functional theory (DFT) calculations were carried out,⁷⁹⁻⁸¹ as this approach has proven to be very reliable for ^{17}O NMR spectral assignments in various systems.^{13-15, 20-21, 24} Although the calculated δ_{iso} value may not exactly match the experimental value, assignments of multiple signals based on relative calculated δ_{iso} values are typically valid.^{13-15, 20-21, 24} Accordingly, calculated δ_{iso} values were utilized for the assignment of each signal in the F1 dimension (Table 1) to the framework oxygen site(s). For example, the order of calculated δ_{iso} values for $\mu^2\text{-O}$ sites in as-made $\alpha\text{-Mg}_3(\text{HCOO})_6$ is O3 < O9 < O1 \approx O11 \approx O5 < O7. The ^{17}O signal with the lowest measured δ_{iso} of 220 ppm ($\delta_1 = 224$ ppm) is thus assigned to O3, the ^{17}O signal with the second-lowest δ_{iso} of 223 ppm ($\delta_1 = 227$ ppm) is assigned to O9, the ^{17}O signal with the third-lowest δ_{iso} of 230 ppm ($\delta_1 = 234$ ppm) and significantly higher intensity is assigned to O1, O5 and O11, and the ^{17}O signal with the highest δ_{iso} of 236 ppm ($\delta_1 = 241$ ppm) is assigned to O7. The ^{17}O signals of $\mu^1\text{-O}$ sites are assigned in a similar fashion. Since the ^{17}O signals at $\delta_1 = 224$ ppm, 227 ppm, and 241 ppm each correspond to a single oxygen site,

their C_Q and η_Q values can be further extracted by fitting the F2 cross-sections (Table 1). The 2D 3QMAS spectrum of activated α - $Mg_3(HCOO)_6$ was analyzed with the same approach and the results are also shown in Table 1.

The spinning sidebands in 1D spectra are particularly intense, suggesting a very large chemical shift anisotropy (CSA) is present at the ultrahigh magnetic field of 35.2 T. Efforts were made to simulate ^{17}O 1D MAS spectra to estimate the ^{17}O CSA. Theoretically, fitting a 1D MAS spectrum with 12 sites requires 96 independent parameters if both the EFG and CSA effects are considered. Therefore, to practically simulate the spectrum, some approximations must be employed to reduce the number of fitting parameters. Thus, the experimental C_Q , η_Q , and δ_{iso} values of oxygen sites that were resolved in the F1 dimension (e.g., O2, O3, O7, and O9 sites of as-made phase) were directly used in simulations without adjustment. For oxygen sites that are unresolved in the F1 dimension (e.g., O1, O5, and O11 sites of as-made phase), the P_Q and δ_{iso} are average values. However, it is evident from the lineshape of cross-sections that these sites give rise to very similar NMR parameters. For the 1D spectral simulations, the calculated η_Q values (Table S2) were used without further adjustment and the corresponding C_Q values were obtained from the known relationship between P_Q and C_Q/η_Q . The δ_{iso} values were obtained using the average δ_{iso} as a starting point and making slight adjustments. Keeping the C_Q and η_Q constant during the simulation is reasonable as the anisotropy from the EFG is much smaller compared to the CSA at the ultrahigh magnetic field. The small variation of the EFG parameters among different sites contributes very little to the intensity of the SSBs (Figure S8).

To include the CSA effects, additional NMR parameters must be incorporated: two CSA parameters including the reduced anisotropy η_{CS} and the chemical shift asymmetry parameter η_{CS} , along with three Euler angles (ϕ , χ , ψ) describing the orientations of the chemical shift tensor with respect to the EFG tensor principal axis frame (see Experimental).⁷³ It is reasonable to assume that the 6 μ^1 -O sites have the same η_{CS} , since they reside in very similar chemical environments and the η_{CS} value for all 6 μ^2 -O sites have the same value yet are distinct from that of μ^1 -O sites. The η_{CS} values for μ^1 -O and μ^2 -O were modified during simulations, but the calculated η_{CS} values and Euler angles (Table S2) were kept constant.

The final simulated 1D MAS spectra are shown in Figure 3, illustrating that the isotropic regions and SSBs can be simulated reasonably well by considering both the quadrupolar and the CSA effects (see Table S3 for the final NMR parameters for simulation). If only the second-order quadrupolar interaction is considered, the isotropic regions of ^{17}O signals can still be simulated accurately, but the simulated SSBs are far too low in intensity (Figure S8). It is also worth noting that there is a very weak ^{17}O signal at $\delta_1 = 305$ ppm ($P_Q = 9.1$ MHz, $\delta_{iso} = 298$ ppm) in the 3QMAS spectrum. The signal position suggests that it arises from DMF molecules within MOF channels.⁸⁴ Apparently, DMF oxygen atoms are also subject to ^{17}O exchange under the reaction conditions. The enhanced sensitivity and resolution of ^{17}O SSNMR at 35.2 T permit detection of the DMF signal, thus it was included in the simulation of 1D MAS spectrum of as-made α - $Mg_3(HCOO)_6$ (i.e., the O1S site).

In general, the calculated δ_{iso} values are slightly overestimated compared to experimental values. Several factors can be responsible for these discrepancies, including (i) limitations of the GIPAW method, (ii) possible inaccuracy of the crystal structure, (iii) temperature effects on the crystal structure, and (iv) dynamics within the crystal structure.⁸⁵ In this case, the single crystal structures are based on the XRD data obtained at 100 K. In addition, our DFT calculations do not consider molecular motions such as the librational motions of formate anions reported for the related β -Ca(HCOO)₂ at room temperature,⁸⁶ while NMR experiments are subject to their influence.

¹⁷O 2D 3QMAS experiments at an ultrahigh magnetic field strength of 35.2 T has unlocked the identification of twelve inequivalent framework oxygen sites in both the as-made and activated phases of α -Mg₃(HCOO)₆. The experimental P_Q and δ_{iso} values of μ^1 -O sites range from 7.5 to 8.8 MHz and 273 to 297 ppm, respectively; these ranges are 6.6 to 7.8 MHz and 220 to 236 ppm for μ^2 -O sites. Both sets of these ranges are typical for C=O and C—O environments of carboxylates.^{3, 8}

The very high resolution achieved at 35.2 T permits observation of small changes in ¹⁷O NMR parameters such as δ_{iso} at each oxygen site upon activation, which were not observable at a lower field of 21.1 T. Such changes reflect the influence and interaction of guest DMF solvent molecules with the MOF host. Activation of the as-made α -Mg₃(HCOO)₆ phase, and corresponding removal of DMF molecules from the pores, only results in subtle changes in local bond angles and distances while long-range order is preserved.⁶⁰ A comparison between the experimental ¹⁷O δ_{iso} values of as-made and activated α -Mg₃(HCOO)₆ phases reveals that more significant changes occur at μ^1 -O sites versus μ^2 -O sites. This disparity in local structural changes is because each μ^2 -O site is firmly anchored to the framework by two Mg and one C atoms, thus the degree of perturbation on their local oxygen coordination spheres by guest molecules is not as evident as the coordination spheres of μ^1 -O sites, which are only bound to the framework via one Mg and one C atom. The most significant activation-induced changes are associated with the δ_{iso} values of O4 and O10 (> 15 ppm). Figure 4 illustrates the orderly arrangement of DMF molecules along the zig-zag channels of α -Mg₃(HCOO)₆. Each DMF molecule interacts with two adjacent framework formate anions containing O4 and O10 sites. According to the criteria for the formation of O...H—C nonconventional hydrogen bonds (O...H distance < 2.72 Å and O...H—C angle > 130°),⁸⁷ both the O1S...H5 distance of 2.38 Å and the O1S...H5—C5 bond angle of 157° in as-made α -Mg₃(HCOO)₆ are in favor of weak hydrogen bonding. Thus, the significant change in the δ_{iso} value of O10, bound to C5 via a C— μ^1 -O bond, is due to the O1S...H5—C5 hydrogen bonding interaction. In the case of O4, although both the O1S...H2 distance of 2.83 Å and the O1S...H2—C2 bond angle of 88° are not very favorable for O1S...H2—C2 hydrogen bond formation, the O1S...C2 distance of 3.00 Å is considerably shorter than the summation of their van der Waals radii (3.22 Å),⁸⁸ pointing toward van der Waals forces between O1S and C2 as responsible for the significant change in the δ_{iso} value of O4 upon activation.

The formation of O1S...H5—C5 hydrogen bond is also evident from the δ_{iso} value of the DMF amide oxygen site (O1S) in as-made α -Mg₃(HCOO)₆. As demonstrated in the literature,⁸⁴ the δ_{iso} value of the DMF amide oxygen in the absence of hydrogen bonding is

323 ppm, and this value decreases with increasing hydrogen bonding strength. The δ_{iso} value of 298 ppm for O1S corresponds to a hydrogen bonding strength between those of infinitely diluted DMF in ethanol (299.3 ppm) and infinitely diluted DMF in methanol (292.5 ppm).⁸⁴ It is the high sensitivity and high resolution achieved at an ultrahigh field of 35.2 T that make it possible to detect the site-specific O...H—C nonconventional hydrogen bonding involving O10 and O1S and estimate the strength of this interaction. As mentioned earlier, nonconventional O...H—C hydrogen bonding can play important roles in the host–guest interactions in BioMOFs or MOF-based drug delivery systems.^{49–51} Thus, the ability to detect this type of weak interaction and estimate its strength by ¹⁷O SSNMR at ultrahigh field, as demonstrated in this study, provides researchers a useful tool for investigating this type of host–guest interaction in MOF systems.

To further demonstrate the power of ultrahigh magnetic field on MOF characterization using ¹⁷O SSNMR, we examined two activated MOF MIL-53(Al) samples. MIL-53(Al) is a well-studied MOF with high thermal and chemical stability, and is very promising in guest separation.⁸⁹ As Figure 5a illustrates, the channels of as-made MIL-53(Al) are occupied by the unreacted linker precursor molecules, 1,4-benzenedicarboxylic acid (H₂BDC). After activation, the channel dimension increases from $7.3 \times 7.7 \text{ \AA}^2$ to $8.5 \times 8.5 \text{ \AA}^2$ due to the removal of the hydrogen bonding interaction between H₂BDC and the carboxylate of BDC²⁻ linkers in the framework. Upon activation, the framework topology is retained, but the crystal symmetry changes from *Pnma* in the as-made phase to *Imma* in the activated phase.⁴⁷ There are two reports on ¹⁷O SSNMR studies of MIL-53 conducted at lower magnetic fields.^{16–17}

Activation of MIL-53 is not very straightforward. Early on, activation of as-made MIL-53(Al) was performed by directly calcination in air at 503 K for 3 days.⁴⁷ The conditions were harsh and led to the reduced crystallinity. To avoid such harsh activation conditions, a milder alternate route was developed by first exchanging the trapped H₂BDC with DMF under solvothermal conditions (e.g., 423 K) for an extended period (e.g., 12 h or longer) and then heating the DMF-exchanged MOF at 473 K under dynamic vacuum (1 mbar) overnight.⁸⁹ We prepared two ¹⁷O-enriched MIL-53(Al) samples which were activated under identical conditions except the DMF exchange time (see Section S3): 24 h for Sample A and 12h for Sample B. According to literature, an exchange time of 12 h should be sufficient for the activation of MIL-53(Al).⁹⁰ Although the PXRD patterns of Sample A and B look very similar (Figure S5), the ¹⁷O 1D MAS spectra at 35.2 T of Samples A and B look distinctly different in the carboxylate region (Figure 5a). The spectrum of Sample A exhibits a relatively narrow pattern that can be well fitted with a single set of ¹⁷O NMR parameters (Table S4), indicating that the signal corresponds to a single oxygen site. This is consistent with the crystal structure of the activated phase which only has one carboxylate oxygen site in the unit cell.⁴⁷ Thus, the ¹⁷O MAS spectrum clearly indicates that the sample exchanged with DMF for 24 h is fully activated.

The spectrum of Sample B displays a rather broad profile in the carboxylate region that cannot be simulated by a single oxygen site, implying the existence of multiple carboxylate oxygen environments in this sample. It appears that this MOF sample is only partially-activated. The ¹⁷O 3QMAS spectrum of Sample B obtained at 35.2 T provides detailed

information. A long spectral “ridge” is observed for the carboxylate oxygen sites, implying that the partial activation can contribute to the distributions on the quadrupolar coupling and chemical shift, consequently line broadening. Such a situation is not unexpected since MIL-53(Al) is a flexible MOF that undergoes a phase transition from *Pnma* in the as-made phase to *Imma* upon full activation without breaking any bonds. It appears that Sample B represents an intermediate state between these two phases. Furthermore, the unreacted linker precursors in the channels are disordered and seem to be randomly removed. Nonetheless, five peaks are extracted above the “ridge” at $\delta_1 = 212, 217, 226, 237,$ and 244 ppm, respectively. The corresponding P_Q and δ_{iso} values are shown in Table S4. Based on the δ_{iso} values, the peaks at $\delta_1 = 212$ and 217 ppm are assigned to the —OH and C=O of H₂BDC molecules within the MOF channels, respectively.³³ The signal at $\delta_1 = 237$ ppm is attributed to the oxygen site in the empty channels because its δ_{iso} value (232 ppm) is similar to that of activated MIL-53(Al), while the resonances at $\delta_1 = 226$ and 244 ppm are tentatively assigned to the oxygen sites in the occupied channels with local environments similar to those in as-made MIL-53(Al).¹⁶⁻¹⁷ The high resolution and sensitivity of ¹⁷O NMR gained at 35.2 T not only allow for unambiguously distinguishing partially-activated from fully-activated MIL-53(Al) samples, but also permit observation of several oxygen sites in empty and occupied channels in partially-activated MIL-53(Al).

4. Conclusions

In summary, the very high spectral resolution and sensitivity achieved at an ultrahigh magnetic field of 35.2 T in this work represents an advance in ¹⁷O SSNMR spectroscopy. At 35.2 T, many inequivalent carboxylate oxygen sites have been identified in ¹⁷O SSNMR spectra of both the activated and as-made α -Mg₃(HCOO)₆ MOFs. The very high resolution achieved at 35.2 T enables the observation of subtle changes in ¹⁷O SSNMR spectra of as-made and activated α -Mg₃(HCOO)₆ phases. These alterations arise from weak site-specific interactions between DMF guests and the MOF framework, such as hydrogen bonding and van der Waals forces. The investigation of these weak interactions is important for MOF applications in various fields including gas adsorption and biomedical applications. The advantage of performing ¹⁷O SSNMR experiments at 35.2 T for MOF characterization is further illustrated by activation of MIL-53(Al). The partially- and fully-activated phases of MIL-53(Al) can be unambiguously distinguished. Several oxygen sites with different local environments in the partially-activated phase are tentatively identified.

This work illustrates how a wide variety of organic and inorganic compounds are now viable targets for ¹⁷O SSNMR at an ultrahigh magnetic field of 35.2 T. The sensitivity and resolution afforded at this field strength greatly extend the volume and quality of structural and chemical information available from ¹⁷O SSNMR spectroscopy, as much of this data is unavailable at or below magnetic fields of 21.1 T.

Supplementary Material

Refer to Web version on PubMed Central for supplementary material.

ACKNOWLEDGMENTS

J.X. thanks the financial support from the National Natural Science Foundation of China (Project 21904071) and the Open Funds (KF1818) of the State Key Laboratory of Fine Chemicals. Y.H. thanks the Natural Sciences and Engineering Research Council (NSERC) of Canada for a Discovery Grant. A portion of this work was performed at the NHMFL, which is supported by NSF DMR-1644779 and the State of Florida. In addition, development of the SCH magnet and NMR instrumentation was supported by the NSF (DMR-1039938 and DMR-0603042) and NIH (BTRR 1P41 GM122698). We thank Dr. Victor V. Terskikh at University of Ottawa for acquiring ^{17}O SSNMR spectra at 21.1 T.

REFERENCES

- (1). Ashbrook SE; Smith ME, Solid State ^{17}O NMR - An Introduction to the Background Principles and Applications to Inorganic Materials. Chem. Soc. Rev 2006, 35 (8), 718–735. [PubMed: 16862272]
- (2). Brownbill NJ; Gajan D; Lesage A; Emsley L; Blanc F, Oxygen-17 Dynamic Nuclear Polarisation Enhanced Solid-State NMR Spectroscopy at 18.8 T. Chem. Commun 2017, 53, 2563–2566.
- (3). Wu G, Solid-State ^{17}O NMR Studies of Organic and Biological Molecules. Prog. Nucl. Magn. Reson. Spectrosc 2008, 52 (2-3), 118–169.
- (4). Yamada K, Chapter 3 - Recent Applications of Solid-State ^{17}O NMR. Annu. Rep. NMR Spectrosc 2010, 70, 115–158.
- (5). Gerothanassis IP, Oxygen-17 NMR Spectroscopy: Basic Principles and Applications (Part II). Prog. Nucl. Magn. Reson. Spectrosc 2010, 57 (1), 1–110. [PubMed: 20633360]
- (6). Castiglione F; Mele A; Raos G, Chapter Four - ^{17}O NMR: A “Rare and Sensitive” Probe of Molecular Interactions and Dynamics. Annu. Rep. NMR Spectrosc 2015, 85, 143–193.
- (7). Ohlin CA; Casey WH, Chapter Five - ^{17}O NMR as a Tool in Discrete Metal Oxide Cluster Chemistry. Annu. Rep. NMR Spectrosc 2018, 94, 187–248.
- (8). Wu G, ^{17}O NMR Studies of Organic and Biological Molecules in Aqueous Solution and in the Solid State. Prog. Nucl. Magn. Reson. Spectrosc 2019, 114–115, 135–191. [PubMed: 31779879]
- (9). Buannic L; Blanc F; Middlemiss DS; Grey CP, Probing Cation and Vacancy Ordering in the Dry and Hydrated Yttrium-Substituted BaSnO_3 Perovskite by NMR Spectroscopy and First Principles Calculations: Implications for Proton Mobility. J. Am. Chem. Soc 2012, 134 (35), 14483–14498. [PubMed: 22691062]
- (10). Wang WD; Lucier BEG; Terskikh VV; Wang W; Huang Y, Wobbling and Hopping: Studying Dynamics of CO_2 Adsorbed in Metal–Organic Frameworks via ^{17}O Solid-State NMR. J. Phys. Chem. Lett 2014, 5 (19), 3360–3365. [PubMed: 26278445]
- (11). Holmes ST; Schurko RW, Refining Crystal Structures with Quadrupolar NMR and Dispersion-Corrected Density Functional Theory. J. Phys. Chem. C 2017, 122 (3), 1809–1820.
- (12). Alam TM; Nyman M; Cherry BR; Segall JM; Lybarger LE, Multinuclear NMR Investigations of the Oxygen, Water, and Hydroxyl Environments in Sodium Hexaniobate. J. Am. Chem. Soc 2004, 126 (17), 5610–5620. [PubMed: 15113233]
- (13). Pedone A; Gambuzzi E; Menziani MC, Unambiguous Description of the Oxygen Environment in Multicomponent Aluminosilicate Glasses from ^{17}O Solid State NMR Computational Spectroscopy. J. Phys. Chem. C 2012, 116 (27), 14599–14609.
- (14). Romao CP; Perras FA; Werner-Zwanziger U; Lussier JA; Miller KJ; Calahoo CM; Zwanziger JW; Bieringer M; Marinkovic BA; Bryce DL; White MA, Zero Thermal Expansion in $\text{ZrMgMo}_3\text{O}_{12}$: NMR Crystallography Reveals Origins of Thermoelastic Properties. Chem. Mater 2015, 27 (7), 2633–2646.
- (15). Kong X; Terskikh VV; Khade RL; Yang L; Rorick A; Zhang Y; He P; Huang Y; Wu G, Solid-State ^{17}O NMR Spectroscopy of Paramagnetic Coordination Compounds. Angew. Chem. Int. Ed 2015, 54 (16), 4753–4757.
- (16). He P; Xu J; Terskikh VV; Sutrisno A; Nie H-Y; Huang Y, Identification of Nonequivalent Framework Oxygen Species in Metal–Organic Frameworks by ^{17}O Solid-State NMR. J. Phys. Chem. C 2013, 117 (33), 16953–16960.

- (17). Bignami GPM; Davis ZH; Dawson DM; Morris SA; Russell SE; McKay D; Parke RE; Iuga D; Morris RE; Ashbrook SE, Cost-Effective ^{17}O Enrichment and NMR Spectroscopy of Mixed-Metal Terephthalate Metal-Organic Frameworks. *Chem. Sci* 2018, 9, 850–859. [PubMed: 29629152]
- (18). Chen C-H; Gaillard E; Mentink-Vigier F; Chen K; Gan Z; Gaveau P; Rebière B; Berthelot R; Florian P; Bonhomme C; Smith ME; Métro T-X; Alonso B; Laurencin D, Direct ^{17}O Isotopic Labeling of Oxides Using Mechanochemistry. *Inorg. Chem* 2020, doi: 10.1021/acs.inorgchem.0c00208.
- (19). Champouret Y; Coppel Y; Kahn ML, Evidence for Core Oxygen Dynamics and Exchange in Metal Oxide Nanocrystals from In Situ ^{17}O MAS NMR. *J. Am. Chem. Soc* 2016, 138 (50), 16322–16328. [PubMed: 27998089]
- (20). Wang M; Wu X-P; Zheng S; Zhao L; Li L; Shen L; Gao Y; Xue N; Guo X; Huang W; Gan Z; Blanc F; Yu Z; Ke X; Ding W; Gong X-Q; Grey CP; Peng L, Identification of Different Oxygen Species in Oxide Nanostructures with ^{17}O Solid-State NMR Spectroscopy. *Sci. Adv* 2015, 1 (1), e1400133. [PubMed: 26601133]
- (21). Métro T-X; Gervais C; Martinez A; Bonhomme C; Laurencin D, Unleashing the Potential of ^{17}O NMR Spectroscopy Using Mechanochemistry. *Angew. Chem. Int. Ed* 2017, 56 (24), 6803–6807.
- (22). Griffin JM; Clark L; Seymour VR; Aldous DW; Dawson DM; Iuga D; Morris RE; Ashbrook SE, Ionothermal ^{17}O Enrichment of Oxides Using Microlitre Quantities of Labelled Water. *Chem. Sci* 2012, 3 (7), 2293–2300.
- (23). Trease NM; Clark TM; Grandinetti PJ; Stebbins JF; Sen S, Bond Length-Bond Angle Correlation in Densified Silica—Results from ^{17}O NMR Spectroscopy. *J. Chem. Phys* 2017, 146 (18), 184505.
- (24). Pavón E; Osuna FJ; Alba MD; Delevoye L, Natural Abundance ^{17}O MAS NMR and DFT Simulations: New Insights into the Atomic Structure of Designed Micas. *Solid State Nucl. Magn. Reson* 2019, 100, 45–51. [PubMed: 30927718]
- (25). Pustogow A; Luo Y; Chronister A; Su YS; Sokolov DA; Jerzembeck F; Mackenzie AP; Hicks CW; Kikugawa N; Raghu S; Bauer ED; Brown SE, Constraints on the Superconducting Order Parameter in Sr_2RuO_4 from Oxygen-17 Nuclear Magnetic Resonance. *Nature* 2019, 574 (7776), 72–75. [PubMed: 31548658]
- (26). Peng L; Liu Y; Kim N; Readman JE; Grey CP, Detection of Bronsted Acid Sites in Zeolite HY with High-Field ^{17}O -MAS-NMR Techniques. *Nat. Mater* 2005, 4 (3), 216–219. [PubMed: 15711551]
- (27). Hung I; Uldry A-C; Becker-Baldus J; Webber AL; Wong A; Smith ME; Joyce SA; Yates JR; Pickard CJ; Dupree R; Brown SP, Probing Heteronuclear ^{15}N — ^{17}O and ^{13}C — ^{17}O Connectivities and Proximities by Solid-State NMR Spectroscopy. *J. Am. Chem. Soc* 2009, 131 (5), 1820–1834. [PubMed: 19138069]
- (28). Chen L; Lu X; Wang Q; Lafon O; Trébosc J; Deng F; Amoureux J-P, Distance Measurement between A Spin-1/2 and A Half-Integer Quadrupolar Nuclei by Solid-State NMR Using Exact Analytical Expressions. *J. Magn. Reson* 2010, 206 (2), 269–273. [PubMed: 20678947]
- (29). Carnahan SL; Lampkin BJ; Naik P; Hanrahan MP; Slowing II; VanVeller B; Wu G; Rossini AJ, Probing O—H Bonding through Proton Detected ^1H — ^{17}O Double Resonance Solid-State NMR Spectroscopy. *J. Am. Chem. Soc* 2019, 141 (1), 441–450. [PubMed: 30525547]
- (30). Jakobsen HJ; Bildsøe H; Brorson M; Wu G; Gor'kov PL; Gan Z; Hung I, High-Field ^{17}O MAS NMR Reveals $^1\text{J}(^{17}\text{O}\text{--}^{127}\text{I})$ with its Sign and the NMR Crystallography of the Scheelite Structures for NaIO_4 and KIO_4 . *J. Phys. Chem. C* 2015, 119 (25), 14434–14442.
- (31). Perras FA; Kobayashi T; Pruski M, Natural Abundance ^{17}O DNP Two-Dimensional and Surface-Enhanced NMR Spectroscopy. *J. Am. Chem. Soc* 2015, 137 (26), 8336–8339. [PubMed: 26098846]
- (32). Harris RK; Becker ED; Cabral De Menezes SM; Goodfellow R; Granger P, NMR Nomenclature. Nuclear Spin Properties and Conventions for Chemical Shifts (IUPAC Recommendations 2001). *Pure Appl. Chem* 2001, 73 (11), 1795–1818.
- (33). Gan Z; Hung I; Wang X; Paulino J; Wu G; Litvak IM; Gor'kov PL; Brey WW; Lendi P; Schiano JL; Bird MD; Dixon IR; Toth J; Boebinger GS; Cross TA, NMR Spectroscopy up to 35.2 T

Using A Series-Connected Hybrid Magnet. *J. Magn. Reson* 2017, 284, 125–136. [PubMed: 28890288]

- (34). Keeler EG; Michaelis VK; Colvin MT; Hung I; Gor'kov PL; Cross TA; Gan Z; Griffin RG, ¹⁷O MAS NMR Correlation Spectroscopy at High Magnetic Fields. *J. Am. Chem. Soc.* 2017, 139 (49), 17953–17963. [PubMed: 29111706]
- (35). Keeler EG; Michaelis VK; Wilson CB; Hung I; Wang X; Gan Z; Griffin RG, High-Resolution ¹⁷O NMR Spectroscopy of Structural Water. *J. Phys. Chem. B* 2019, 123 (14), 3061–3067. [PubMed: 30882222]
- (36). Zhou H-C; Long JR; Yaghi OM, Introduction to Metal–Organic Frameworks. *Chem. Rev* 2012, 112 (2), 673–674. [PubMed: 22280456]
- (37). Furukawa H; Cordova KE; O'Keeffe M; Yaghi OM, The Chemistry and Applications of Metal–Organic Frameworks. *Science* 2013, 341 (6149), 1230444. [PubMed: 23990564]
- (38). Hoffmann HC; Debowski M; Mueller P; Paasch S; Senkowska I; Kaskel S; Brunner E, Solid-State NMR Spectroscopy of Metal–Organic Framework Compounds (MOFs). *Materials* 2012, 5, 2537–2572.
- (39). Sutrisno A; Huang Y, Solid-State NMR: A Powerful Tool for Characterization of Metal–Organic Frameworks. *Solid State Nucl. Magn. Reson* 2013, 49–50, 1–11.
- (40). Lucier BEG; Chen S; Huang Y, Characterization of Metal–Organic Frameworks: Unlocking the Potential of Solid-State NMR. *Acc. Chem. Res* 2018, 51 (2), 319–330. [PubMed: 29251909]
- (41). Witherspoon VJ; Xu J; Reimer JA, Solid-State NMR Investigations of Carbon Dioxide Gas in Metal–Organic Frameworks: Insights into Molecular Motion and Adsorptive Behavior. *Chem. Rev* 2018, 118 (20), 10033–10048. [PubMed: 30288971]
- (42). Wong YTA; Martins V; Lucier BEG; Huang Y, Solid-State NMR Spectroscopy: A Powerful Technique to Directly Study Small Gas Molecules Adsorbed in Metal–Organic Frameworks. *Chem. –Eur. J* 2019, 25 (8), 1848–1853. [PubMed: 30189105]
- (43). Lucier BEG; Zhang Y; Huang Y, Complete Multinuclear Solid-State NMR of Metal–Organic Frameworks: The Case of α -Mg-formate. *Concept. Magnetic Res. A* 2016, 45A (6), e21410.
- (44). Lucier BEG; Zhang Y; Lee KJ; Lu Y; Huang Y, Grasping Hydrogen Adsorption and Dynamics in Metal–Organic Frameworks Using ²H Solid-State NMR. *Chem. Commun* 2016, 52 (48), 7541–7544.
- (45). Lu Y; Lucier B; Zhang Y; Ren P; Zheng A; Huang Y, Sizable Dynamics in Small Pores: CO₂ Location and Motion in the α -Mg Formate Metal–Organic Framework. *Phys. Chem. Chem. Phys* 2017, 19, 6130–6141. [PubMed: 28191584]
- (46). Zhang Y; Lucier BEG; Fischer M; Gan Z; Boyle PD; Desveaux B; Huang Y, A Multifaceted Study of Methane Adsorption in Metal–Organic Frameworks by Using Three Complementary Techniques. *Chem. –Eur. J* 2018, 24 (31), 7866–7881. [PubMed: 29575184]
- (47). Loiseau T; Serre C; Huguénard C; Fink G; Taulelle F; Henry M; Bataille T; Férey G, A Rationale for the Large Breathing of the Porous Aluminum Terephthalate (MIL-53) upon Hydration. *Chem. –Eur. J* 2004, 10 (6), 1373–1382. [PubMed: 15034882]
- (48). Kitagawa S; Uemura K, Dynamic Porous Properties of Coordination Polymers Inspired by Hydrogen Bonds. *Chem. Soc. Rev* 2005, 34 (2), 109–119. [PubMed: 15672175]
- (49). McKinlay AC; Morris RE; Horcajada P; Férey G; Gref R; Couvreur P; Serre C, BioMOFs: Metal–Organic Frameworks for Biological and Medical Applications. *Angew. Chem. Int. Ed* 2010, 49 (36), 6260–6266.
- (50). Cai H; Huang Y-L; Li D, Biological Metal–Organic Frameworks: Structures, Host–Guest Chemistry and Bio-Applications. *Coord. Chem. Rev* 2019, 378, 207–221.
- (51). Wu M-X; Yang Y-W, Metal–Organic Framework (MOF)-Based Drug/Cargo Delivery and Cancer Therapy. *Adv. Mater* 2017, 29 (23), 1606134.
- (52). Li H; Eddaoudi M; O'Keeffe M; Yaghi M, Design and Synthesis of an Exceptionally Stable and Highly Porous Metal–Organic Framework. *Nature* 1999, 402 (6759), 276–279.
- (53). Millange F; Serre C; Férey G, Synthesis, Structure Determination and Properties of MIL-53as and MIL-53ht: The First Cr^{III} Hybrid Inorganic–Organic Microporous Solids: Cr^{III}(OH)·{O₂C–C₆H₄–CO₂}·{HO₂C–C₆H₄–CO₂H}_x. *Chem. Commun* 2002, 2002 (8), 822–823.

- (54). Hafizovic Cavka J; Jakobsen S; Olsbye U; Guillou N; Lamberti C; Bordiga S; Lillerud KP, A New Zirconium Inorganic Building Brick Forming Metal Organic Frameworks with Exceptional Stability. *J. Am. Chem. Soc* 2008, 130 (42), 13850–13851. [PubMed: 18817383]
- (55). Rosi NL; Kim J; Eddaoudi M; Chen B; O'Keeffe M; Yaghi OM, Rod Packings and Metal–Organic Frameworks Constructed from Rod-Shaped Secondary Building Units. *J. Am. Chem. Soc* 2005, 127 (5), 1504–1518. [PubMed: 15686384]
- (56). Chui SS-Y; Lo SM-F; Charmant JPH; Orpen AG; Williams ID, A Chemically Functionalizable Nanoporous Material $[\text{Cu}_3(\text{TMA})_2(\text{H}_2\text{O})_3]_n$. *Science* 1999, 283 (5405), 1148–1150. [PubMed: 10024237]
- (57). Ahmed I; Jung SH, Applications of Metal–Organic Frameworks in Adsorption/Separation Processes via Hydrogen Bonding Interactions. *Chem. Eng. J* 2017, 310, 197–215.
- (58). Roberts JM; Fini BM; Sarjeant AA; Farha OK; Hupp JT; Scheidt KA, Urea Metal–Organic Frameworks as Effective and Size-Selective Hydrogen–Bond Catalysts. *J. Am. Chem. Soc* 2012, 134 (7), 3334–3337. [PubMed: 22296523]
- (59). Meng X; Wang H-N; Song S-Y; Zhang H-J, Proton-Conducting Crystalline Porous Materials. *Chem. Soc. Rev* 2017, 46 (2), 464–480. [PubMed: 27918056]
- (60). Rood JA; Noll BC; Henderson KW, Synthesis, Structural Characterization, Gas Sorption and Guest-Exchange Studies of the Lightweight, Porous Metal–Organic Framework α - $[\text{Mg}_3(\text{O}_2\text{CH})_6]$. *Inorg. Chem* 2006, 45 (14), 5521–5528. [PubMed: 16813415]
- (61). Fischer M; Hoffmann F; Froeba M, New Microporous Materials for Acetylene Storage and $\text{C}_2\text{H}_2/\text{CO}_2$ Separation: Insights from Molecular Simulations. *ChemPhysChem* 2010, 11 (10), 2220–2229. [PubMed: 20540140]
- (62). Lian X; Fang Y; Joseph E; Wang Q; Li J; Banerjee S; Lollar C; Wang X; Zhou H-C, Enzyme–MOF (Metal–Organic Framework) Composites. *Chem. Soc. Rev* 2017, 46 (11), 3386–3401. [PubMed: 28451673]
- (63). Novio F; Simmchen J; Vázquez-Mera N; Amorín-Ferré L; Ruiz-Molina D, Coordination Polymer Nanoparticles in Medicine. *Coord. Chem. Rev* 2013, 257 (19), 2839–2847.
- (64). Xu J; Terskikh VV; Chu Y; Zheng A; Huang Y, Mapping Out Chemically Similar, Crystallographically Nonequivalent Hydrogen Sites in Metal–Organic Frameworks by ^1H Solid-State NMR Spectroscopy. *Chem. Mater* 2015, 27 (9), 3306–3316.
- (65). Hu J; Sun T; Ren X; Wang S, HF-Assisted Synthesis of Ultra-Microporous $[\text{Mg}_3(\text{OOCH})_6]$ Frameworks for Selective Adsorption of CH_4 over N_2 . *Microporous Mesoporous Mater.* 2015, 204, 73–80.
- (66). Xu J; Terskikh VV; Huang Y, Resolving Multiple Non-equivalent Metal Sites in Magnesium-Containing Metal–Organic Frameworks by Natural Abundance ^{25}Mg Solid-State NMR Spectroscopy. *Chem. –Eur. J* 2013, 19 (14), 4432–4436. [PubMed: 23450828]
- (67). Mao H; Xu J; Hu Y; Huang Y; Song Y, The Effect of High External Pressure on Structure and Stability of MOF α - $\text{Mg}_3(\text{HCOO})_6$ Probed by in Situ Raman and FT-IR Spectroscopy. *J. Mater. Chem. A* 2015, 3, 11976–11984.
- (68). Xu J; Terskikh VV; Chu Y; Zheng A; Huang Y, ^{13}C Chemical Shift Tensors in MOF α - $\text{Mg}_3(\text{HCOO})_6$: Which Component is More Sensitive to Host-Guest Interaction? *Magn. Reson. Chem* 2020, doi: 10.1002/mrc.4944.
- (69). Toby BH; Von Dreele RB, GSAS-II: The Genesis of a Modern Open-Source All Purpose Crystallography Software Package. *J. Appl. Crystallogr* 2013, 46 (2), 544–549.
- (70). Rood JA; Henderson KW, Synthesis and Small Molecule Exchange Studies of a Magnesium Bisformate Metal–Organic Framework: An Experiment in Host-Guest Chemistry for the Undergraduate Laboratory. *J. Chem. Educ* 2013, 90 (3), 379–382.
- (71). Massiot D; Touzo B; Trumeau D; Coutures JP; Virlet J; Florian P; Grandinetti PJ, Two-Dimensional Magic-Angle Spinning Isotropic Reconstruction Sequences for Quadrupolar Nuclei. *Solid State Nucl. Magn. Reson* 1996, 6 (1), 73–83. [PubMed: 8925268]
- (72). Hung I; Trébosc J; Hoatson GL; Vold RL; Amoureux J-P; Gan Z, Q-Shear Transformation for MQMAS and STMAS NMR Spectra. *J. Magn. Reson* 2009, 201 (1), 81–86. [PubMed: 19733107]

- (73). Massiot D; Fayon F; Capron M; King I; Le Calve S; Alonso B; Durand J-O; Bujoli B; Gan Z; Hoatson G, Modeling One- and Two-Dimensional Solid-State NMR Spectra. *Magn. Reson. Chem* 2002, 40 (1), 70–76.
- (74). Kresse G; Hafner J, *Ab Initio* Molecular-Dynamics Simulation of the Liquid-Metal--Amorphous-Semiconductor Transition in Germanium. *Phys. Rev. B* 1994, 49 (20), 14251–14269.
- (75). Giannozzi P; Baroni S; Bonini N; Calandra M; Car R; Cavazzoni C; Ceresoli D; Chiarotti GL; Cococcioni M; Dabo I; Dal Corso A; de Gironcoli S; Fabris S; Fratesi G; Gebauer R; Gerstmann U; Gougoussis C; Kokalj A; Lazzeri M; Martin-Samos L; Marzari N; Mauri F; Mazzarello R; Paolini S; Pasquarello A; Paulatto L; Sbraccia C; Scandolo S; Sclauzero G; Seitsonen AP; Smogunov A; Umari P; Wentzcovitch RM, QUANTUM ESPRESSO: A Modular and Open-Source Software Project for Quantum Simulations of Materials. *J. Phys.: Condens. Matter* 2009, 21 (39), 395502. [PubMed: 21832390]
- (76). Perdew JP; Burke K; Ernzerhof M, Generalized Gradient Approximation Made Simple. *Phys. Rev. Lett* 1996, 77 (18), 3865–3868. [PubMed: 10062328]
- (77). Troullier N; Martins JL, Efficient Pseudopotentials for Plane-Wave Calculations. *Phys. Rev. B* 1991, 43 (3), 1993–2006.
- (78). Kleinman L; Bylander DM, Efficacious Form for Model Pseudopotentials. *Phys. Rev. Lett* 1982, 48 (20), 1425–1428.
- (79). Charpentier T, The PAW/GIPAW Approach for Computing NMR Parameters: A New Dimension Added to NMR Study of Solids. *Solid State Nucl. Magn. Reson* 2011, 40 (1), 1–20. [PubMed: 21612895]
- (80). Bonhomme C; Gervais C; Babonneau F; Coelho C; Pourpoint F; Azaïs T; Ashbrook SE; Griffin JM; Yates JR; Mauri F; Pickard CJ, First-Principles Calculation of NMR Parameters Using the Gauge Including Projector Augmented Wave Method: A Chemist's Point of View. *Chem. Rev* 2012, 112 (11), 5733–5779. [PubMed: 23113537]
- (81). Pickard CJ; Mauri F, All-Electron Magnetic Response with Pseudopotentials: NMR Chemical Shifts. *Phys. Rev. B* 2001, 63 (24), 245101.
- (82). Frydman L; Harwood JS, Isotropic Spectra of Half-Integer Quadrupolar Spins from Bidimensional Magic-Angle Spinning NMR. *J. Am. Chem. Soc* 1995, 117 (19), 5367–5368.
- (83). Amoureux J-P; Huguenard C; Engelke F; Taulelle F, Unified Representation of MQMAS and STMAS NMR of Half-Integer Quadrupolar Nuclei. *Chem. Phys. Lett* 2002, 356 (5), 497–504.
- (84). Gerothanassis IP; Vakka C, ¹⁷O NMR Chemical Shifts as a Tool to Study Specific Hydration Sites of Amides and Peptides: Correlation with the IR Amide I Stretching Vibration. *J. Org. Chem* 1994, 59 (9), 2341–2348.
- (85). Michaelis VK; Keeler EG; Ong T-C; Craigen KN; Penzel S; Wren JEC; Kroeker S; Griffin RG, Structural Insights into Bound Water in Crystalline Amino Acids: Experimental and Theoretical ¹⁷O NMR. *J. Phys. Chem. B* 2015, 119 (25), 8024–8036. [PubMed: 25996165]
- (86). Hallock KJ; Lee DK; Ramamoorthy A, The Effects of Librations on the ¹³C Chemical Shift and ²H Electric Field Gradient Tensors in β -Calcium Formate. *J. Chem. Phys* 2000, 113 (24), 11187–11193.
- (87). Desiraju GR; Steiner T, *The Weak Hydrogen Bond in Structural Chemistry and Biology*. Oxford University Press: Oxford/New York, 1999.
- (88). Bondi A, van der Waals Volumes and Radii. *J. Phys. Chem* 1964, 68 (3), 441–451.
- (89). Trung TK; Trens P; Tanchoux N; Bourrelly S; Llewellyn PL; Loera-Serna S; Serre C; Loiseau T; Fajula F; Férey G, Hydrocarbon Adsorption in the Flexible Metal Organic Frameworks MIL-53(Al, Cr). *J. Am. Chem. Soc* 2008, 130 (50), 16926–16932. [PubMed: 19053405]
- (90). Zhang Y; Lucier BEG; Huang Y, Deducing CO₂ Motion, Adsorption Locations and Binding Strengths in a Flexible Metal–Organic Framework without Open Metal Sites. *Phys. Chem. Chem. Phys* 2016, 18 (12), 8327–8341. [PubMed: 26427010]

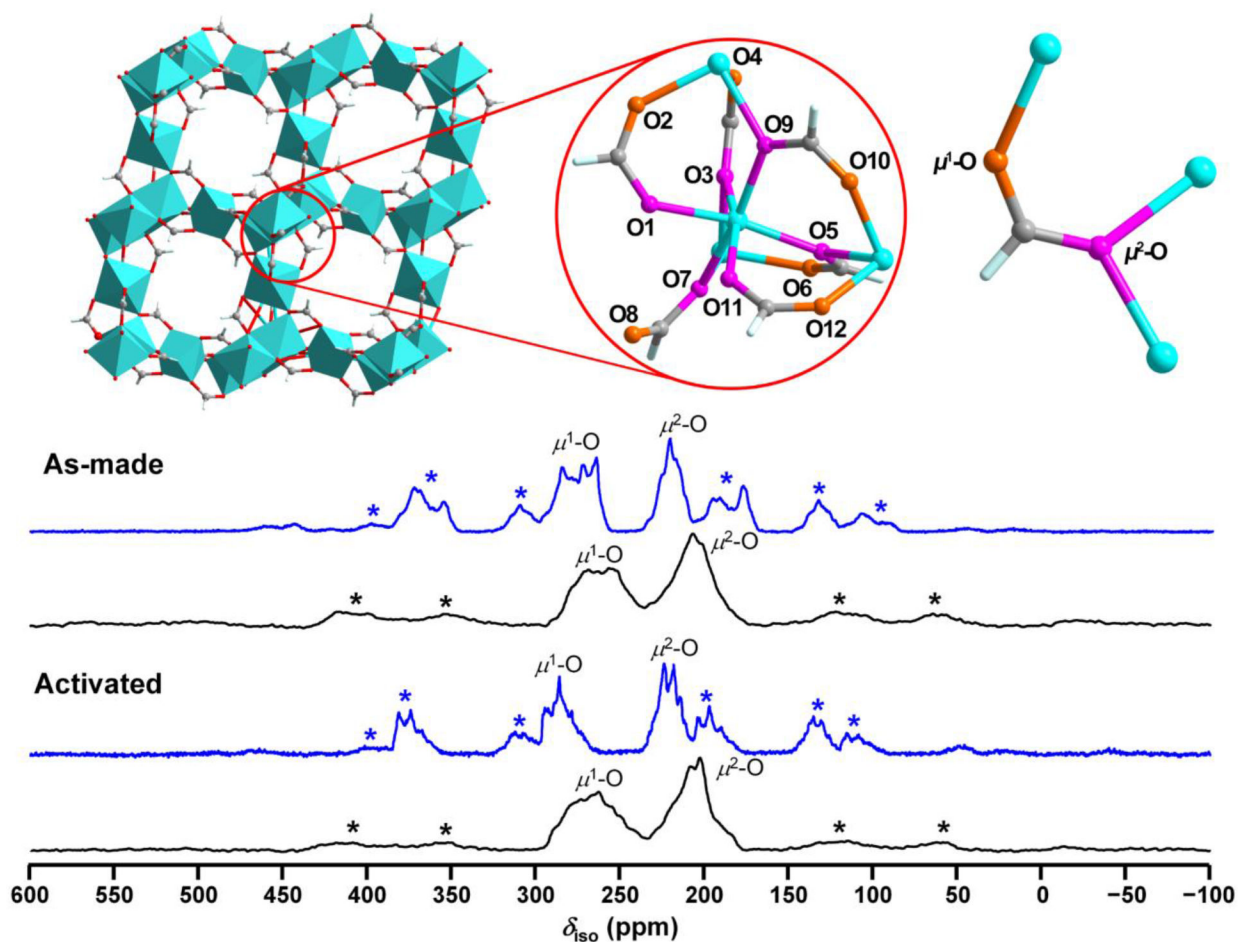


Figure 1.

Top (left to right): Representations of the framework of activated α - $\text{Mg}_3(\text{HCOO})_6$, twelve framework oxygen sites, and two different oxygen bonding modes. Color coding: Mg, turquoise; C, grey; H, white; O, red; μ^1 -O, orange; μ^2 -O, pink. **Bottom:** ^{17}O 1D MAS NMR spectra of ^{17}O -enriched α - $\text{Mg}_3(\text{HCOO})_6$ at fields of 35.2 T (blue) and 21.1 T (black) acquired at a spinning frequency of 18 kHz. The asterisk (*) denotes spinning sidebands (SSBs). The ^{17}O 1D MAS NMR spectrum of as-made α - $\text{Mg}_3(\text{HCOO})_6$ at 21.1 T is adapted with permission from the American Chemical Society.¹⁶

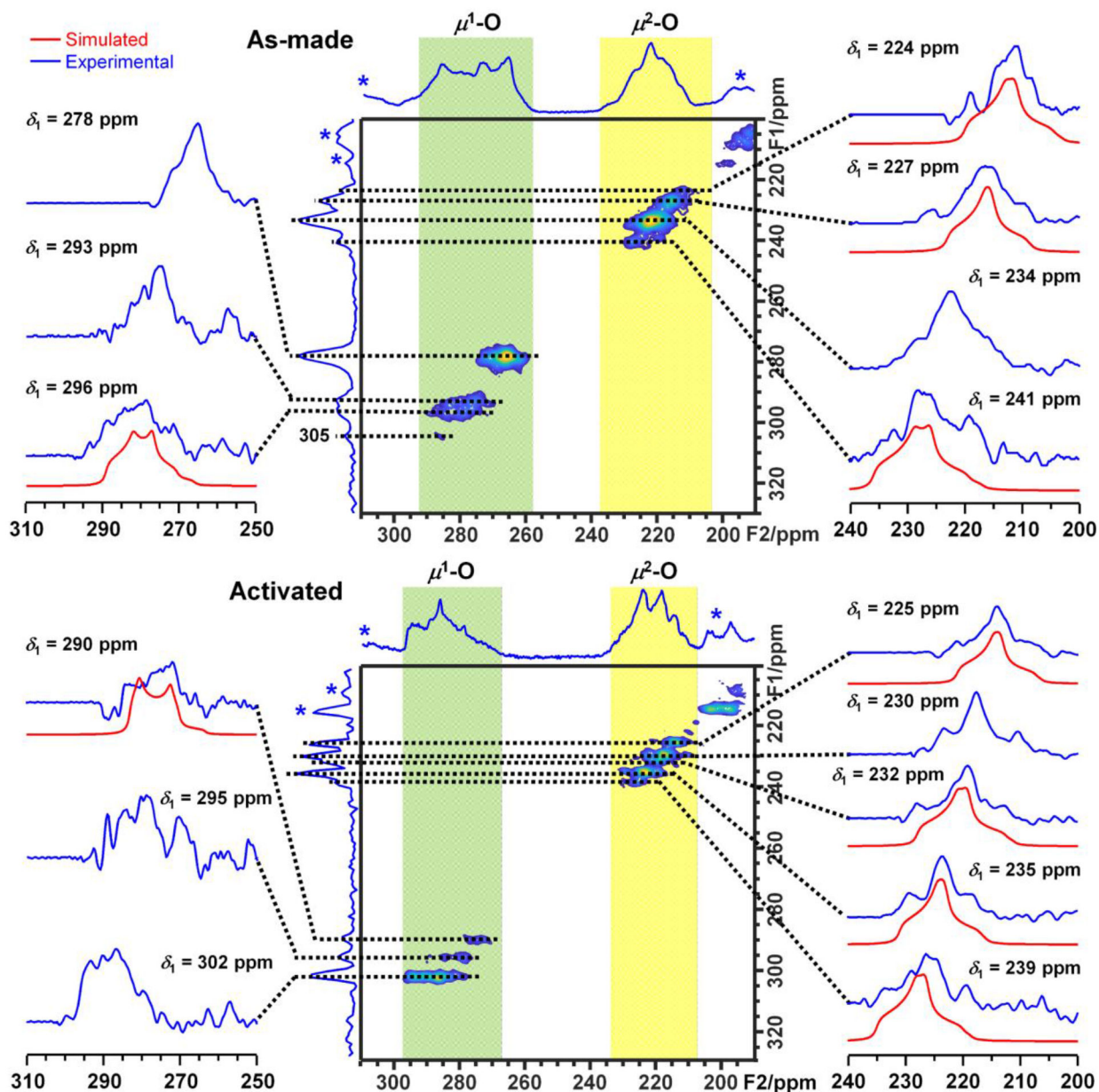


Figure 2.

^{17}O 2D 3QMAS NMR spectra of ^{17}O -enriched $\alpha\text{-Mg}_3(\text{HCOO})_6$ at 35.2 T. Black dashed lines correspond to the slices examined. Blue and red solid lines denote experimental and simulated spectra, respectively. The asterisk (*) denotes the SSBs. The 3QMAS spectra were acquired using a shifted-echo MQMAS pulse sequence and rotor synchronized t_1 , and processed using the Q-shearing method to avoid spectral folding of the peaks and SSBs.⁷² The 3QMAS spectra without markups are shown in Figure S7 for clarity.

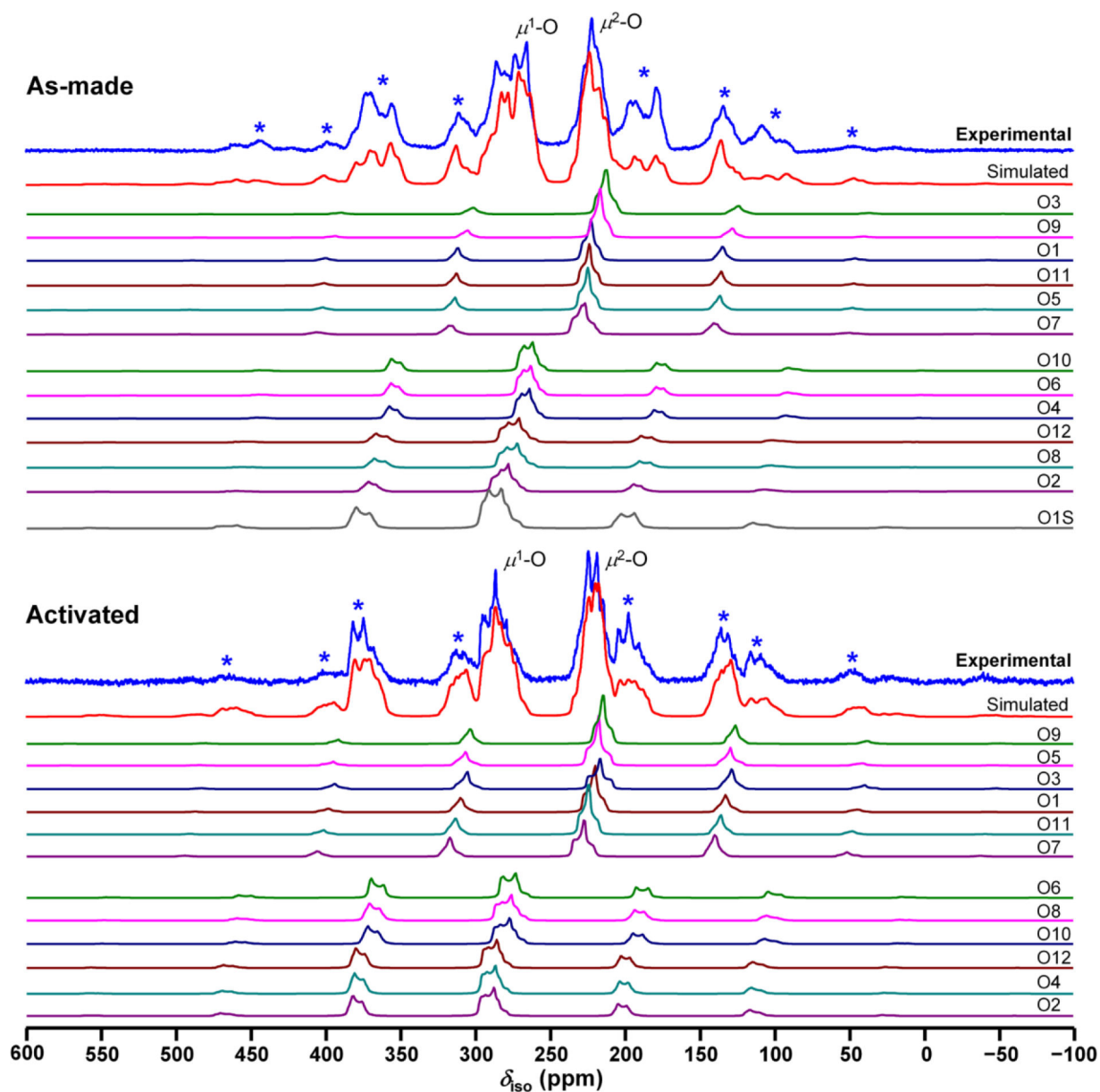


Figure 3. Experimental and simulated ^{17}O 1D MAS NMR spectra of ^{17}O -enriched $\alpha\text{-Mg}_3(\text{HCOO})_6$ at 35.2 T. Both the quadrupolar and CSA effects are considered in these simulations, using the parameters shown in Table S3. In each phase, the signal intensity of each individual oxygen in the $\mu^1\text{-O}$ sites is approximately equal, and the same is true for signals arising from the $\mu^2\text{-O}$ sites. The asterisk (*) denotes SSBs.

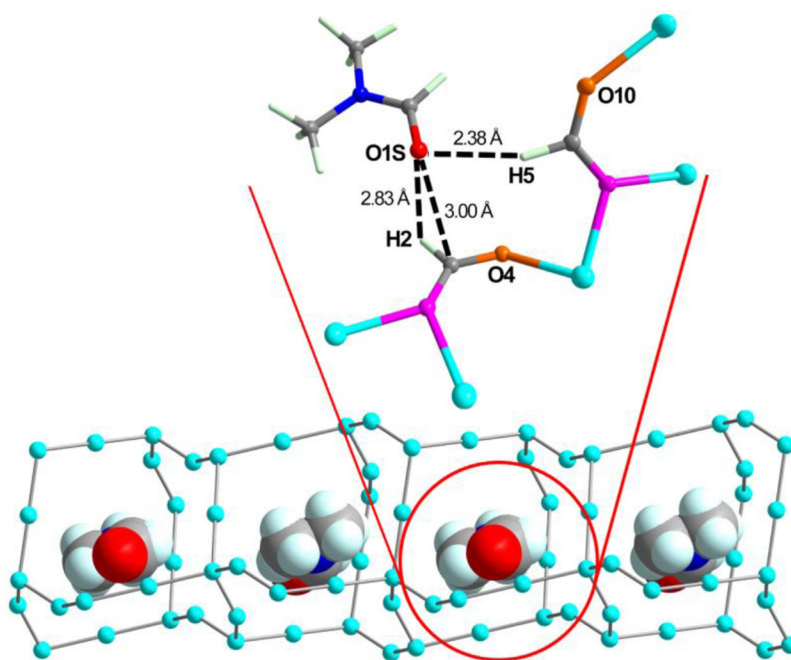


Figure 4. Schematic illustrations of DMF guest molecules within the zig-zag channels of as-made α - $\text{Mg}_3(\text{HCOO})_6$. Only the Mg nodes are shown for clarity in the bottom diagram. The top inset shows a DMF molecule and two adjacent formate anions. The distances listed were extracted from the DFT-optimized structures. Color coding: Mg, turquoise; N, blue; C, grey; H, white; O1S of DMF, red; μ^1 -O, orange; μ^2 -O, pink.

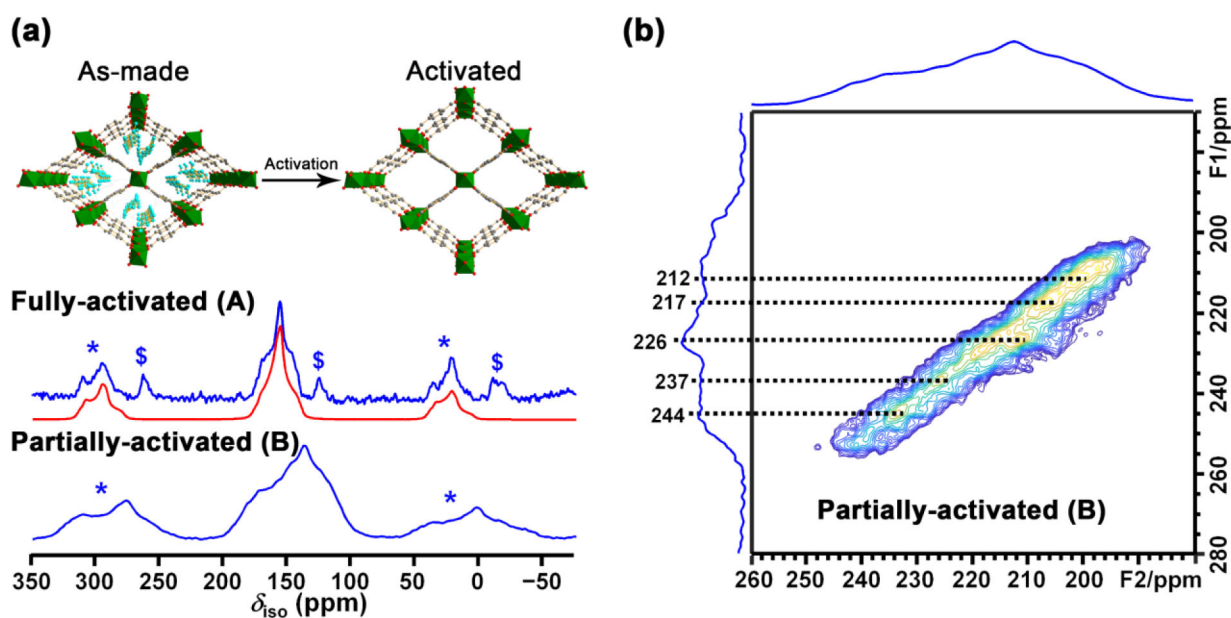


Figure 5.

(a) ^{17}O 1D MAS NMR spectra of ^{17}O -enriched fully- (Sample A) and partially- (Sample B) activated MIL-53(Al) samples at 35.2 T. The blue and red solid lines denote experimental and simulated spectra, respectively. Only the carboxylate oxygen regions are shown for clarity. The full spectra are shown in Figure S9. The asterisk (*) and dollar sign (\$) denotes the SSBs of $-\text{COO}^-$ and $\mu^2\text{-OH}$, respectively. The structures of as-made and activated MIL-53(Al) phases are shown at top. (b) ^{17}O 2D 3QMAS NMR spectrum of partially-activated (Sample B) ^{17}O -enriched MIL-53(Al) at 35.2 T. Black dashed lines correspond to the slices examined for analyses.

Table 1.Experimental ^{17}O NMR parameters, calculated^a δ_{iso} values, and peak assignments of $\alpha\text{-Mg}_3(\text{HCOO})_6$.

Sample	O Type	δ_1 (ppm)	P_Q (MHz)	δ_{iso} (ppm)	$\delta_{\text{iso, calc}}$ (ppm)	Assignment	C_Q (MHz)	η_Q
As-made	$\mu^2\text{-O}$	224(1)	7.2(5)	220(2)	227.1	O3	6.5(4)	0.80(10)
		227(1)	6.6(5)	223(2)	230.5	O9	6.0(4)	0.88(10)
		234(1)	6.6(5)	230(2)	236.1	O1		
					238.9	O11		
					239.4	O5		
	$\mu^2\text{-O}$	241(1)	7.8(5)	236(2)	256.4	O7	7.0(4)	0.70(10)
	$\mu^1\text{-O}$	278(1)	7.5(5)	273(2)	288.7	O10		
					291.2	O6		
					293.2	O4		
	$\mu^1\text{-O}$	293(1)	8.8(5)	286(2)	295.5	O12		
					297.2	O8		
	$\mu^1\text{-O}$	296(1)	8.3(5)	290(2)	306.5	O2	7.9(4)	0.55(10)
DMF	305(1)	9.1(5)	298(2)	308.3	O1S			
Activated	$\mu^2\text{-O}$	225(1)	6.6(5)	221(2)	227.7	O9	6.0(4)	0.85(10)
		230(1)	7.5(5)	225(2)	232.0	O3		
				232.0	O5			
	$\mu^2\text{-O}$	232(1)	7.2(5)	228(2)	234.7	O1	6.5(4)	0.80(10)
	$\mu^2\text{-O}$	235(1)	6.9(5)	231(2)	238.7	O11	6.1(4)	0.85(10)
	$\mu^2\text{-O}$	239(1)	7.2(5)	235(2)	243.5	O7	6.4(4)	0.80(10)
	$\mu^1\text{-O}$	290(1)	7.8(5)	285(2)	285.3	O6	7.7(4)	0.20(10)
	$\mu^1\text{-O}$	295(1)	8.1(5)	289(2)	288.0	O8		
					289.9	O10		
	$\mu^1\text{-O}$	302(1)	7.5(5)	297(2)	296.4	O12		
				296.5	O4			
				298.5	O2			

The numbers in the parentheses are the estimated uncertainty of the last significant figure.

^aThe complete calculated ^{17}O NMR parameters are shown in Table S2.